HHS Public Access

Author manuscript

J Magn Reson Imaging. Author manuscript; available in PMC 2017 August 01.

Published in final edited form as:

J Magn Reson Imaging. 2016 August ; 44(2): 317–326. doi:10.1002/jmri.25171.

Assessment of Renal Function Using Intravoxel Incoherent Motion Diffusion-Weighted Imaging and Dynamic Contrast-Enhanced MRI

Octavia Bane, PhD[1], **Mathilde Wagner, MD PhD**[1], **Jeff L. Zhang, PhD**[4], **Hadrien A. Dyvorne, PhD**[1], **Matthew Orton, PhD**[5], **Henry Rusinek, PhD**[3], and **Bachir Taouli, MD**[1,2]

[1]Translational and Molecular Imaging Institute, Icahn School of Medicine at Mount Sinai, New York, NY

[2]Department of Radiology, Icahn School of Medicine at Mount Sinai, New York, NY

[3]Departments of Radiology and Biomedical Engineering, New York University, New York, NY

[4]Departments of Radiology and Biomedical Engineering, University of Utah, Salt Lake City, UT

[5]Division of Radiotherapy and Imaging, Institute of Cancer Research, Sutton, Surrey, UK

Abstract

Objective—To assess the correlation between each of intravoxel incoherent motion diffusion-weighted imaging (IVIM-DWI) and dynamic contrast-enhanced MRI (DCE-MRI) metrics in renal parenchyma with renal function, in a cohort of patients with chronic liver disease.

Materials and Methods—Thirty patients with liver disease underwent abdominal MRI at 1.5T, including a respiratory-triggered IVIM-DWI sequence and a coronal 3D FLASH DCE-MRI acquisition. Diffusion signals in the renal cortex and medulla were fitted to the IVIM model to estimate the diffusion coefficient (D), pseudodiffusion coefficient (D*) and perfusion fraction (PF). Apparent diffusion coefficient (ADC) was calculated using all b-values. GFR, cortical and medullary renal plasma flow (RPF), mean transit times (MTT) of vascular and tubular compartments and the whole kidney, were calculated from DCE-MRI data by fitting to a three-compartment model. eGFR was calculated from serum creatinine measured 30 ± 27 days of MRI.

Results—ADC, PF, and RPF were significantly higher in renal cortex vs medulla ($p < 10^{-5}$). DCE-MRI GFR significantly correlated with, but under-estimated eGFR (Spearman's r/p=0.49/0.01). IVIM-DWI parameters were not significantly correlated with eGFR. DCE-MRI GFR correlated weakly with D (cortex, r/p=0.3/0.03; medulla r/p=0.27/0.05) and ADC (cortex r/p=0.28/0.04; medulla r/p=0.34/0.01). Weak correlations were observed for pooled cortical and medullar RPF with PF (r/p=0.32/10^{-3}) and with ADC (r/p=0.29/0.0025). Significant negative correlations were observed for vascular MTT with cortical D* (r/p=−0.38/0.004) and D*×PF (r/p=−0.34/0.01).

Corresponding Author: Bachir Taouli, MD, Icahn School of Medicine at Mount Sinai, Department of Radiology and Translational and Molecular Imaging Institute, One Gustave L Levy Place, Box 1234, New York, NY 10029 USA, bachir.taouli@mountsinai.org, Tel: (212) 824-8453, Fax: 646-537-9589.

Conclusion—The weak correlations between renal IVIM and DCE-MRI perfusion parameters imply that these functional measures could be complementary.

Keywords

renal DCE-MRI; renal DWI-MRI; IVIM; renal function in liver disease

INTRODUCTION

MRI provides an accurate assessment of renal morphology, as well as of vascular or obstructive renal disorders. However, functional renal impairment often precedes anatomical changes, such as thinning of the cortex or decrease of kidney size (1). The most commonly used assessment of renal function, the estimated glomerular filtration rate (eGFR) obtained from serum creatinine, is insensitive to the early stages of renal dysfunction, and confounded by co-morbidities associated with liver disease in which the level of serum creatinine is low despite moderate to severe renal dysfunction (2). Moreover, eGFR only assesses global kidney function, and does not provide independent assessment of each kidney.

Functional MRI techniques such as intravoxel incoherent motion diffusion-weighted imaging (IVIM-DWI) and dynamic contrast-enhanced MRI (DCE-MRI) have the potential to assess renal dysfunction. Tissue microstructure might be characterized by the apparent diffusion coefficient (ADC), which is estimated from DWI signals with mono-exponential function (1,3,4). A reduction in ADC has been observed in renal dysfunction, and attributed to either reduced water reabsorption or renal fibrosis restricting water diffusion (1,5,6). The ability of IVIM to separate the effect on signal of molecular diffusion from that of capillary perfusion is readily apparent in the kidney, as parameters reflecting perfusion (ADC, pseudodiffusion coefficient D* and perfusion fraction PF) have been shown to have higher values in the more perfused renal cortex (1) than in the renal medulla (5,7). Thus, IVIM analysis for the cortex and the medulla separately, rather than for the whole kidney, has the potential to assess different aspects of renal physiology (e.g. vascular perfusion and water reabsorption, dominant in the cortex, vs. tubular flow, dominant in the medulla) (1).

DCE-MRI images the passage of a bolus of exogenous contrast agent through the tissues of interest, with high temporal resolution. Mathematical models are then used to calculate the tracer concentration from signal changes and then to quantify tissue perfusion and distribution volume of the tracer. There are several tracer kinetic models of the kidney, from simple clearance models (8,9) to dual compartment models accounting for excretion of tracer from renal tubules (10), to three-compartment (3C) models describing structures in the cortex and medulla as serially connected compartments (2,11). The 3C model provides values of GFR and renal plasma flow (RPF) that correlated strongly with Tc^{99m}-DTPA clearance measurements in patients with renal dysfunction (12), and better precision than two-compartment models (13).

Overall, there is emerging consensus that IVIM and DCE-MRI techniques enable more complex modeling of renal water transport and function, without the limitations of creatinine-based eGFR (2), while being less expensive and time consuming than clearance methods, without radiation involved as in radionuclide renography (1). However, high

quality data is crucial for greater precision in parameter estimation with both techniques. Respiratory motion diminishes data quality during lengthy IVIM or DCE-MRI abdominal acquisitions. Modern algorithms for co-registration of volumetric time series (4D) data specifically developed for abdominal organs can be used to correct for respiratory motion (14,15).

Our primary objective was to study, in the clinical setting, the correlations between renal function parameters derived from IVIM diffusion and 3C DCE-MRI models, so as to determine whether IVIM related perfusion parameters might be used as surrogates of perfusion in the kidney. Our focus is on patients with liver disease because the evaluation of renal function by serum eGFR alone in patients with advanced liver disease (cirrhosis) can provide misleading results (2). Our secondary objective is to correlate IVIM and DCE-MRI metrics to renal function, as measured by serum eGFR.

PATIENTS AND METHODS

Patients

Eighty-four patients with chronic liver disease underwent abdominal MRI as part of a prospective single-center study. The project was approved by the local IRB and written informed consent was obtained from all subjects. Among this population, patients with coronal renal IVIM-DWI and DCE-MRI data and with eGFR measurement less than 90 days before the MRI were included in the current study. None of the patients had history of acute or chronic renal dysfunction. The number of patients excluded and reasons for exclusion are detailed in Fig. 1. Finally, 30 patients were included (M/F 20/10, mean age 58 y, range 42–69 y) with liver disease of various etiologies [chronic hepatitis C (n=24), non-alcoholic steatohepatitis (n=4), chronic hepatitis B (n=1), primary biliary cirrhosis (n=1)]. Liver biopsy was available for 26/30 patients for evaluation of fibrosis stage and inflammation, according to the METAVIR (16) and Brunt (17) scoring systems. Liver cirrhosis was confirmed in 3 of 4 patients without biopsy, based on clinical and imaging findings (two were liver transplant candidates and one underwent a transjugular intrahepatic shunt procedure) (18). Eight patients had liver cirrhosis, and 22 were not cirrhotic. All 8 patients with cirrhosis had compensated cirrhosis. For all patients, eGFR was calculated by the Cockroft-Gault equation from serum creatinine measurements taken within 90 days of MRI (mean delay 30 ± 27 d, range 0–84 d).

Image acquisition

All patients were instructed to fast for 4 hours before the MRI. Patients were imaged on a 1.5T system (Magnetom Avanto, Siemens Healthcare, Erlangen, Germany) equipped with a multichannel spine and body matrix coil and 45 mT/m maximum gradient strength. Axial and coronal T_2-weighted (T2WI) HASTE, axial fat-suppressed T2WI, axial dual-echo chemical shift imaging, coronal IVIM-DWI and DCE-MRI were performed.

IVIM-DWI—A bipolar diffusion sequence with single-shot EPI readout and spectral fat saturation was acquired, in 17 interleaved slices covering the abdomen in the coronal plane (Table 1) (3). The acquisition was respiratory triggered, controlled by a 5 mm coronal

navigator slice placed on the dome of the liver, with an acceptance window of 2 mm. Images were acquired with 16 b-values (0, 15, 30, 45, 60, 75, 90, 105, 120, 135, 150, 175, 200, 400, 600, and 800 s/mm^2) in order to sample both the initial IVIM pseudodiffusion decay (b <200 s/mm^2) and the molecular diffusion decay (b ≥200 s/mm^2). Each non-zero b-value was prescribed in three orthogonal diffusion directions, which were combined into a mean diffusivity-weighted image using a three-pass trace in image reconstruction.

DCE-MRI—data consisted of 64 coronal abdominal 3D volumes acquired using a 3D FLASH sequence, with mean temporal resolution of 2.7 s (Table 1). A bolus of 0.05 mmol/kg of Gd-BOPTA (gadobenate dimeglumine; MultiHance, Bracco Diagnostics Inc., Italy) was injected intravenously, followed by a 25 ml saline flush; both were injected at 5 ml/s (19,20). The injection was performed with an 8 sec time delay, so that 3 of 64 abdominal volumes were acquired before contrast injection. The total acquisition time was 2.5–4 minutes (19). The coronal orientation and a small flip angle were selected to minimize aortic inflow effects. Patients were instructed to hold their breath for 40 s, and then for several intervals of 24 s during the DCE-MRI acquisition, with breath holds separated by short periods (6.6 s) of quick breathing (19).

Image analysis

Image analysis was performed by two observers in consensus (observer 1, O.B, a MRI physicist with 7 years of experience, and observer 2, M.W., a body radiologist with 4 years of experience). Both observers were blinded to the GFR and the liver disease status of the patients.

IVIM-DWI—Motion artifact in the IVIM data was corrected by affine 2D registration to the images of the lowest b-value, performed for each kidney separately using the locally developed software FireVoxel (CAI2R, New York University, New York, NY) (14) (15,21) (Fig. 2). Freehand ROIs were delineated bilaterally, in the cortex and medulla, on two perihilar slices. Cortical ROIs (5–10 cm^3) followed the outer contour of the kidney, avoiding artifacts, major vessels and lesions (Fig. 2). Medullary ROIs (Fig. 2; 3–6 ROIs/slice; 5–10 cm^3) were traced using T_2-weighted anatomical images and the arterial phase of DCE-MR image as reference, avoiding artifacts, major vessels, lesions and renal fat. Signals were averaged for all voxels inside ROI of same type, and were then fitted by a Bayesian algorithm to the IVIM equation 1 (7), to obtain the diffusion coefficient D (10^{-3} mm^2/s), the pseudodiffusion coefficient D* (10^{-3} mm^2/s), and the perfusion fraction PF (%) (3,7). ADC (10^{-3} mm^2/s) was obtained from monoexponential fit of mean ROI signal to equation 2, for all 16 b-values. IVIM parameters and ADC values were averaged between the two slices.

$$S=S_0[PF\cdot e^{-b\cdot D^*}+(1-PF)\cdot e^{-b\cdot D}] \quad \text{(Equation 1)}$$

$$S=S_0\cdot e^{-b\cdot ADC} \quad \text{(Equation 2)}$$

DCE-MRI—The cropped images for each kidney were corrected for motion artifact by automatic registration with manual correction, and the cortex, medulla and collecting system in each kidney were semi-automatically segmented into volume ROIs using a previously validated segmentation software (----) developed in C++ (22). The aorta at the level of the renal arteries was also semi-automatically segmented to measure arterial input function. The signal intensities averaged for the ROIs were converted to contrast concentration using the FLASH equation and baseline T_1 values for the blood and renal tissues based on literature values (12) (Fig. 3). Concentration versus time curves of renal tissue were fitted in Matlab R2015 (Mathworks, Natick, MA) by a nonlinear least-squares algorithm to the previously validated three-compartment model (2,11,12). The model describes the flow of renal plasma with contrast agent from the aortic input to the arterial compartment (at rate RPF in ml/min), after which a portion of plasma is filtered at the rate of GFR into the proximal tubule and then loop of Henle (12). With the model, GFR, cortical and medullary RPF, and mean transit times (MTT) for each individual compartment and the whole kidney, can be estimated from contrast concentration vs. time curves of kidneys.

Simulation of IVIM-DWI variability with offset from isocenter

It is well known that actual b-values differ from nominal b-values at the location of the kidneys (± 10 cm from isocenter), due to gradient non-linearity (23–25). We assumed that the ratio of actual to nominal b-value varies with the square of the gradient amplitude, according to equation 3 (23). Furthermore, we assume that this ratio at ± 10 cm from isocenter on the right to left axis has the same value at 1.5T as at 3T. Since gradient non-linearity was found to be more pronounced at 3T, this is a conservative assumption (23).

$$\frac{b_{\text{actual}}}{b_{\text{nominal}}} \sim \left(\frac{G_{\text{actual}}}{G_{\text{nominal}}}\right)^2 = 1.06 \quad \text{(Equation 3)}$$

For a set of population-based IVIM parameters for the medulla and cortex, we simulated noiseless IVIM signal at the location of the kidneys using 16 actual b-values. We then fitted the signal to the 16 nominal b-values used in our experiments, to obtain calculated IVIM parameters.

Test-retest reproducibility of IVIM-DWI and DCE-MRI parameters

IVIM-DWI and DCE-MRI parameters were measured in 4 and 2 patients, respectively, who had repeat exams, 7 days apart, by the two observers acting in consensus.

Statistical analysis

DCE-MRI parameters were compared by Spearman correlation to the IVIM parameters, for the right and left kidney, and for averaged values between the kidneys. Pooled medullary and cortical IVIM parameters and RPF for both kidneys were compared to assess whether IVIM parameters reflect renal perfusion. eGFR was also correlated with IVIM and DCE-MRI parameters. Agreement of the DCE-MRI GFR with serum eGFR was assessed by Bland-Altman statistics. Parameters were compared between renal cortex and medulla by Mann-Whitney test. Unpaired Mann-Whitney tests were also used to compare renal IVIM and

DCE-MRI parameters between patients with and without liver cirrhosis. In addition, coefficients of variation (CVs, in %) were used to assess test-retest reproducibility between repeat exams, between right and left kidney, and between IVIM parameters measured at isocenter and at a right/left offset from isocenter.

RESULTS

All 30 patients analyzed for both IVIM-DWI and DCE-MRI metrics had Cockroft-Gault eGFR ≥40 ml/min (mean eGFR 84.6 22.7 ml/min, range 40.5–140.7 ml/min). Four patients had mildly impaired renal function, as denoted by eGFR <60 ml/min.

Estimated IVIM and DCE-MRI parameters

Cortical ADC and PF (Table 2) were significantly higher than in the medulla (p=0.02 and $p<10^{-5}$, respectively), while there was no significant difference for D and D* (p=0.47 and p=0.13, respectively). None of the IVIM parameters correlated significantly with eGFR. There was no significant difference in cortical or medullary IVIM parameters between cirrhotic and non-cirrhotic patients (Mann-Whitney p=0.36–0.98).

The AIF was truncated, preventing DCE-MRI quantification in 3 patients (Table 3). Thus, DCE-MRI parameters were obtained in 27/30 patients. DCE-MRI GFR correlated significantly with eGFR (r=0.49, p=0.01), but was systematically lower than the latter [slope=0.44, p=0.002; intercept=13.12, p=0.245; Bland-Altman mean difference −34 ml/min, 95% limits of agreement (−72, 4) ml/min] (Fig. 4). RPF values (Table 3) were significantly higher in the cortex than in the medulla ($p<10^{-6}$). There was also no significant difference in whole kidney, cortical or medullary DCE-MRI parameters between cirrhotic and non-cirrhotic patients (Mann-Whitney p=0.26–0.93).

Variability of IVIM and DCE-MRI parameters

The CV of IVIM-DWI parameters in test-retest MRI exams 7 days apart, as well as between the left and right kidneys, are given in Table 4. Test-retest CVs in the cortex and medulla CV's were less than 5% for ADC, less than 10% for D, and less than 30% for perfusion-dependent parameters PF and D*. The cortical and medullary CV between left and right kidney for ADC was slightly increased over 5%, and slightly increased over 6% for D, while it was less than 17% for PF and less than 35% for D*.

For DCE-MRI parameters, test-retest CVs (Table 5) were under 30%, with vascular MTT_A the least variable (CV=3.9%), and cortical RPF, the most variable (CV= 25.57%). The CVs between left and right kidneys (Table 5), given for all parameters except GFR (which is a global parameter that takes both kidneys into account), were between 10 (vascular MTT_A) and 25% (whole kidney RPF).

Variability of IVIM parameters with offset from isocenter

For a set of population-based IVIM parameters for the medulla [D (10^{-3} mm^2/s), PF (%), D* (10^{-3} mm^2/s), ADC (10^{-3} mm^2/s)]=[2.0, 15, 40, 2.1], after fitting the simulated signal to the 16 nominal b-values used in our experiments, we obtained the following calculated

parameters [D (10^{-3} mm^2/s), PF (%), D* (10^{-3} mm^2/s), ADC (10^{-3} mm^2/s)]=[2.1, 15.25, 40.9, 2.2]. This resulted in CVs between population-based and calculated parameters of 3.3% (D), 1.2% (PF), 1.5% (D*) and 4.1% (ADC). Repeating the same simulation for the cortex with population-based parameters [D (10^{-3} mm^2/s), PF (%), D* (10^{-3} mm^2/s), ADC (10^{-3} mm^2/s)]=[2.2, 25, 35, 2.4], we obtained the following calculated parameters [D (10^{-3} mm^2/s), PF (%), D* (10^{-3} mm^2/s), ADC (10^{-3} mm^2/s)]=[2.3,25.42,37.1,2.5], with CVs of 3.6% (D), 1.2% (PF), 4.1% (D*) and 4.1% (ADC), all below test-retest CVs.

Correlation between IVIM and DCE-MRI parameters

DCE-MRI GFR (Fig. 5) showed significant but modest correlation with D and ADC of the cortex (D: r=0.3, p=0.03, ADC: r=0.28, p=0.04) and medulla (D: r=0.27, p=0.05, ADC: r=0.34, p=0.01). RPF correlated significantly with PF and ADC for pooled cortical and medullary data (Fig. 5; PF r=0.32, $p=10^{-3}$, ADC r=0.29, p=0.0025). Cortical RPF correlated with ADC (r=0.35, p=0.009), and D (r=0.29, p=0.032), but not with PF. Significant negative correlation (Fig. 5) was observed between vascular MTT and cortical D* (r = −0.38, PF=0.004) and D*×PF (r = −0.34, p=0.01).

DISCUSSION

Previous studies have attempted to elucidate the relationship between functional MRI measures of renal perfusion, diffusion and renal function (2,6,11,12,26,27). While these studies focused on validation and use of either IVIM-DWI or DCE-MRI in the context of renal dysfunction, our study sought to identify areas of overlap and redundancy of the two techniques. Both IVIM-DWI and DCE-MRI examine renal perfusion, although from different aspects (i.e. the effect of blood perfusion on diffusion, versus vascular transport of a filterable tracer). Strong correlation between PF measured by IVIM-DWI and DCE-MRI measures of perfusion (RPF) or filtration (GFR) would promote use of IVIM-DWI as an alternative to DCE-MRI.

IVIM-DWI is well suited to characterize diffusion in highly vascular organs such as the kidney by separating molecular diffusion dependent on tissue structure (D) from pseudodiffusion (D*), dependent on capillary blood velocity. A major challenge to acquiring high-quality DWI data is respiratory motion (1,7). Although our acquisitions have used respiratory triggering to minimize motion artifact, we found coregistration in post-processing was still necessary. Our experience is in accordance to a previous study (7), which showed that a respiratory-triggered IVIM-DWI acquisition does not entirely compensate for respiratory motion in the kidneys.

The renal IVIM parameters obtained in this study were in accordance with a previous study using the Bayesian fit in subjects with normal kidney function and similar range of b-values (7). In other studies of renal IVIM-DWI, parameters were obtained by least-square fitting to the IVIM equation (4,5,26), which describes the signal as a fast pseudodiffusion exponential decay of the vascular fraction PF, dominant at low b-values (b<45 s/mm^2), and a slow exponential decay with constant D of the non-vascular spins, dominant at large b-values (b> 200 s/mm^2 for the kidney) (5). Unlike least-square fitting algorithms, which minimize the residual between the data and the model, Bayesian fitting uses prior distributions of the

parameters to determine a joint posterior probability over all parameters, for the given data. Thus, Bayesian fitting methods provide the probability density function, and thus an estimate of uncertainty for each IVIM parameter, rather than a global coefficient of determination. Previous studies showed that Bayesian fitting is more robust and more accurate for estimating perfusion-dependent parameters than least squares fitting (3,28,29).

We obtained significantly higher PF and ADC in the cortex than in the medulla, which is expected, as the perfusion effect is more prominent in the more vascularized cortex. Higher cortical ADC was observed in two previous studies (5,7), while another study showed higher medullary PF (5). We did not observe significantly higher cortical D or D*, as in previous studies (5,7). These discrepancies between studies are possibly due to differences in b-values, fitting methods [least squares (5) vs Bayesian (7)], and patient populations [healthy volunteers (7) vs. patients with wide range of serum eGFRs (5)].

DCE-MRI parameters measured in our study were in agreement with previous studies using the three-compartment model (12). A significantly higher RPF in the cortex compared to the medulla is expected for the more vascularized cortex. A three-compartment model was chosen, rather than simpler models (Patlak plot, whole-kidney or dual compartment) because it permits separation of cortical and medullary function, and was previously shown to provide information on renal tubular function, and to differentiate between acute rejection and acute tubular necrosis of renal allografts (27). Like previous investigators, we found that the model–derived GFR was systematically lower than serum eGFR (2). Previous comparisons against reference nuclear-medicine measurements found that the model-derived GFR was lower than the reference GFR (12), but was still more accurate than eGFR estimated from serum creatinine (2). Possible explanations of the lower GFR from DCE MRI include: 1) over-estimation of GFR by serum creatinine measurements, especially in patients with liver disease (2); 2) limitations of the three-compartment model, such as the simplified three-compartment description of a complex system, neglecting the effect of intra-extravascular water exchange, and flow effects in the aorta (12).

The high standard deviation in RPF observed in our patient cohort is consistent with similar high uncertainty observed by Zhang et al. in their small group of patients (12). RPF also had the highest test-retest and right to left kidney CVs among DCE-MRI parameters. The high uncertainty/variability of RPF may be due to: 1) high patient-to-patient and right-left kidney physiological variation in renal perfusion, and 2) indirect quantification of the AIF, or concentration of tracer in the aorta, from signal intensity in the aorta, which can be affected by several MR artifacts, such as inflow effect (minimized in coronal orientation), dephasing, partial-volume effect, signal saturation and flow pulsation (1,12).

IVIM parameters derived for our patient group did not correlate significantly with serum eGFR. However, there was significant, but modest positive correlation of DCE-MRI GFR with cortical and medullary D and ADC, which reflect renal structure. The observed relationship between GFR and IVIM parameters is consistent with another study with a larger number of patients and broader range of eGFR (5). In this previous study, significantly lower cortical ADC, D*, and D (5), and medullary D and D* were observed in patient

groups with eGFR ranges of 10–80 ml/min, compared to a control group with normal renal function (eGFR> 80 ml/min).

DCE-MRI RPF and IVIM-DWI PF parameters that characterize capillary perfusion, showed a modest, but significant correlation, for the cortical and medullary data analyzed together. The correlation was not reproduced for PF in the cortex data alone. The correlation between RPF and ADC (for combined data and for the cortex alone) highlights the effect of perfusion on ADC, especially in the well-vascularized cortex. The correlation between RPF and D in the cortex was too modest to infer that there is an effect of cortical structure/diffusion on renal plasma flow. Of note, the significant correlations between vascular MTT with D* and D*×PF (a more robust perfusion parameter than D*), although modest, suggest that slow arterial flow (long vascular MTT) is associated with slower perfusion-dependent decay of the diffusion signal. The modest correlations observed between IVIM-DWI and DCE-MRI parameters do not support the hypothesis that IVIM-DWI parameters can be used as surrogates of DCE-MRI perfusion measurements in the kidney. This precludes the use of IVIM-DWI examination as an alternative to DCE-MRI in patients with contraindications to gadolinium injection.

Our study had several limitations. Our sample size was small, with the majority of patients with normal kidney function (eGFR>60 ml/min, except in four patients, with eGFR between 40 and 60 ml/min). Furthermore, eGFR was measured at a mean of 30 days from the MRI exam, during which values may fluctuate. Because the DWI acquisition was 2D, and the DCE-MRI acquisition was 3D, precise co-registration of the two data sets was not possible. Compared to dedicated renal acquisitions, the coverage of the kidneys was further limited with both abdominal IVIM-DWI and DCE-MRI acquisitions, e.g. 4–10 slices that permitted registration and segmentation of the kidneys. To convert signal to contrast concentration in DCE-MRI analysis, we used literature values of pre-contrast T_1 for blood, renal cortex and renal medulla, since such measurements were not available. For the IVIM-DWI acquisition, the difference between actual and nominal b-value due to gradient non-linearity with offset from isocenter is a well-known limitation. However, our simulation results showed the CV due to b-value difference to be smaller than those obtained between right and left kidneys and below test-retest CV. Lastly, the IVIM model does not distinguish between blood flow and water reabsorption in the renal tubules. A more complex diffusion model is needed to describe renal tubule transport with comparable details to the three-compartment DCE-MRI model.

In conclusion, we observed modest correlations at best between IVIM-DWI and DCE-MRI in the renal cortex and medulla, which suggests that these techniques are complementary and not redundant. A study in a larger number of patients with a wider range of GFRs is needed to validate or invalidate our findings.

Acknowledgments

Grant support:

NIH NIDDK 1R01DK087877

NIBIB NIH P41 EB017183

Société Française de Radiologie

Abbreviations

ADC	apparent diffusion coefficient
D	diffusion coefficient
D*	pseudo diffusion coefficient
DCE-MRI	dynamic contrast-enhanced MRI
DWI	diffusion-weighted imaging
eGFR	estimated glomerular filtration rate
IVIM	intravoxel incoherent motion
MDRD	modification of diet in renal disease
MTT	mean transit time
MTT_A	vascular compartment mean transit time
MTT_P	proximal tubule mean transit time
MTT_L	loop of Henle mean transit time
PF	perfusion fraction
RPF	renal plasma flow

REFERENCES

1. Zhang JL, Rusinek H, Chandarana H, Lee VS. Functional MRI of the kidneys. J Magn Reson Imaging. 2013; 37(2):282–293. [PubMed: 23355431]
2. Vivier PH, Storey P, Rusinek H, et al. Kidney function: glomerular filtration rate measurement with MR renography in patients with cirrhosis. Radiology. 2011; 259(2):462–470. [PubMed: 21386050]
3. Dyvorne HA, Galea N, Nevers T, et al. Diffusion-weighted imaging of the liver with multiple b values: effect of diffusion gradient polarity and breathing acquisition on image quality and intravoxel incoherent motion parameters--a pilot study. Radiology. 2013; 266(3):920–929. [PubMed: 23220895]
4. Le Bihan D, Breton E, Lallemand D, Aubin ML, Vignaud J, Laval-Jeantet M. Separation of diffusion and perfusion in intravoxel incoherent motion MR imaging. Radiology. 1988; 168(2):497–505. [PubMed: 3393671]
5. Ichikawa S, Motosugi U, Ichikawa T, Sano K, Morisaka H, Araki T. Intravoxel incoherent motion imaging of the kidney: alterations in diffusion and perfusion in patients with renal dysfunction. Magn Reson Imaging. 2013; 31(3):414–417. [PubMed: 23102943]
6. Thoeny HC, De Keyzer F, Oyen RH, Peeters RR. Diffusion-weighted MR imaging of kidneys in healthy volunteers and patients with parenchymal diseases: initial experience. Radiology. 2005; 235(3):911–917. [PubMed: 15845792]
7. Jerome NP, Orton MR, d'Arcy JA, Collins DJ, Koh DM, Leach MO. Comparison of free-breathing with navigator-controlled acquisition regimes in abdominal diffusion-weighted magnetic resonance images: Effect on ADC and IVIM statistics. J Magn Reson Imaging. 2014; 39(1):235–240. [PubMed: 23580454]

8. Baumann D, Rudin M. Quantitative assessment of rat kidney function by measuring the clearance of the contrast agent Gd(DOTA) using dynamic MRI. Magn Reson Imaging. 2000; 18(5):587–595. [PubMed: 10913720]
9. Hackstein N, Heckrodt J, Rau WS. Measurement of single-kidney glomerular filtration rate using a contrast-enhanced dynamic gradient-echo sequence and the Rutland-Patlak plot technique. J Magn Reson Imaging. 2003; 18(6):714–725. [PubMed: 14635157]
10. Annet L, Hermoye L, Peeters F, Jamar F, Dehoux JP, Van Beers BE. Glomerular filtration rate: assessment with dynamic contrast-enhanced MRI and a cortical-compartment model in the rabbit kidney. J Magn Reson Imaging. 2004; 20(5):843–849. [PubMed: 15503326]
11. Lee VS, Rusinek H, Bokacheva L, et al. Renal function measurements from MR renography and a simplified multicompartmental model. Am J Physiol Renal Physiol. 2007; 292(5):F1548–F1559. [PubMed: 17213464]
12. Zhang JL, Rusinek H, Bokacheva L, et al. Functional assessment of the kidney from magnetic resonance and computed tomography renography: impulse retention approach to a multicompartment model. Magn Reson Med. 2008; 59(2):278–288. [PubMed: 18228576]
13. Bokacheva L, Rusinek H, Zhang JL, Chen Q, Lee VS. Estimates of glomerular filtration rate from MR renography and tracer kinetic models. J Magn Reson Imaging. 2009; 29(2):371–382. [PubMed: 19161190]
14. Song, T.; Lee, VS.; Rusinek, H.; Kaur, M.; Laine, AF. Automatic 4-D Registration in Dynamic MR Renography. Proceedings of IEEE 2005: Engineering in Medicine and Biology 27th Annual Conference; Shanghai, China. 2005. p. 3067-3070.
15. Mikheev, A.; Lee, VS.; H, R. Targeted coregistration of abdominal DCE MRI. Proceedings of the 19th Scientific Meeting of ISMRM; Montreal, Canada. 2011. (abstract 2578)
16. Bedossa P, Poynard T. An algorithm for the grading of activity in chronic hepatitis C. The METAVIR Cooperative Study Group. Hepatology. 1996; 24(2):289–293. [PubMed: 8690394]
17. Brunt EM, Kleiner DE, Wilson LA, Belt P, Neuschwander-Tetri BA. Nonalcoholic fatty liver disease (NAFLD) activity score and the histopathologic diagnosis in NAFLD: distinct clinicopathologic meanings. Hepatology. 2011; 53(3):810–820. [PubMed: 21319198]
18. Yin M, Glaser KJ, Talwalkar JA, Chen J, Manduca A, Ehman RL. Hepatic MR Elastography: Clinical Performance in a Series of 1377 Consecutive Examinations. Radiology. 2015:142141.
19. Aronhime S, Calcagno C, Jajamovich GH, et al. DCE-MRI of the liver: effect of linear and nonlinear conversions on hepatic perfusion quantification and reproducibility. J Magn Reson Imaging. 2014; 40(1):90–98. [PubMed: 24923476]
20. Jajamovich GH, Calcagno C, Dyvorne HA, Rusinek H, Taouli B. DCE-MRI of the liver: reconstruction of the arterial input function using a low dose pre-bolus contrast injection. PLoS One. 2014; 9(12):e115667. [PubMed: 25546176]
21. Sigmund EE, Vivier PH, Sui D, et al. Intravoxel incoherent motion and diffusion-tensor imaging in renal tissue under hydration and furosemide flow challenges. Radiology. 2012; 263(3):758–769. [PubMed: 22523327]
22. Rusinek H, Boykov Y, Kaur M, et al. Performance of an automated segmentation algorithm for 3D MR renography. Magn Reson Med. 2007; 57(6):1159–1167. [PubMed: 17534915]
23. Malyarenko D, Galban CJ, Londy FJ, et al. Multi-system repeatability and reproducibility of apparent diffusion coefficient measurement using an ice-water phantom. J Magn Reson Imaging. 2013; 37(5):1238–1246. [PubMed: 23023785]
24. Belli G, Busoni S, Ciccarone A, et al. Quality assurance multicenter comparison of different MR scanners for quantitative diffusion-weighted imaging. J Magn Reson Imaging. 2015
25. Malyarenko DI, Newitt D, L JW, et al. Demonstration of nonlinearity bias in the measurement of the apparent diffusion coefficient in multicenter trials. Magn Reson Med. 2015
26. Rheinheimer S, Schneider F, Stieltjes B, et al. IVIM-DWI of transplanted kidneys: reduced diffusion and perfusion dependent on cold ischemia time. Eur J Radiol. 2012; 81(9):e951–e956. [PubMed: 22785337]
27. Yamamoto A, Zhang JL, Rusinek H, et al. Quantitative evaluation of acute renal transplant dysfunction with low-dose three-dimensional MR renography. Radiology. 2011; 260(3):781–789. [PubMed: 21771953]

28. Andreou A, Koh DM, Collins DJ, et al. Measurement reproducibility of perfusion fraction and pseudodiffusion coefficient derived by intravoxel incoherent motion diffusion-weighted MR imaging in normal liver and metastases. Eur Radiol. 2013; 23(2):428–434. [PubMed: 23052642]

29. Neil JJ, Bretthorst GL. On the use of Bayesian probability theory for analysis of exponential decay data: an example taken from intravoxel incoherent motion experiments. Magn Reson Med. 1993; 29(5):642–647. [PubMed: 8505900]

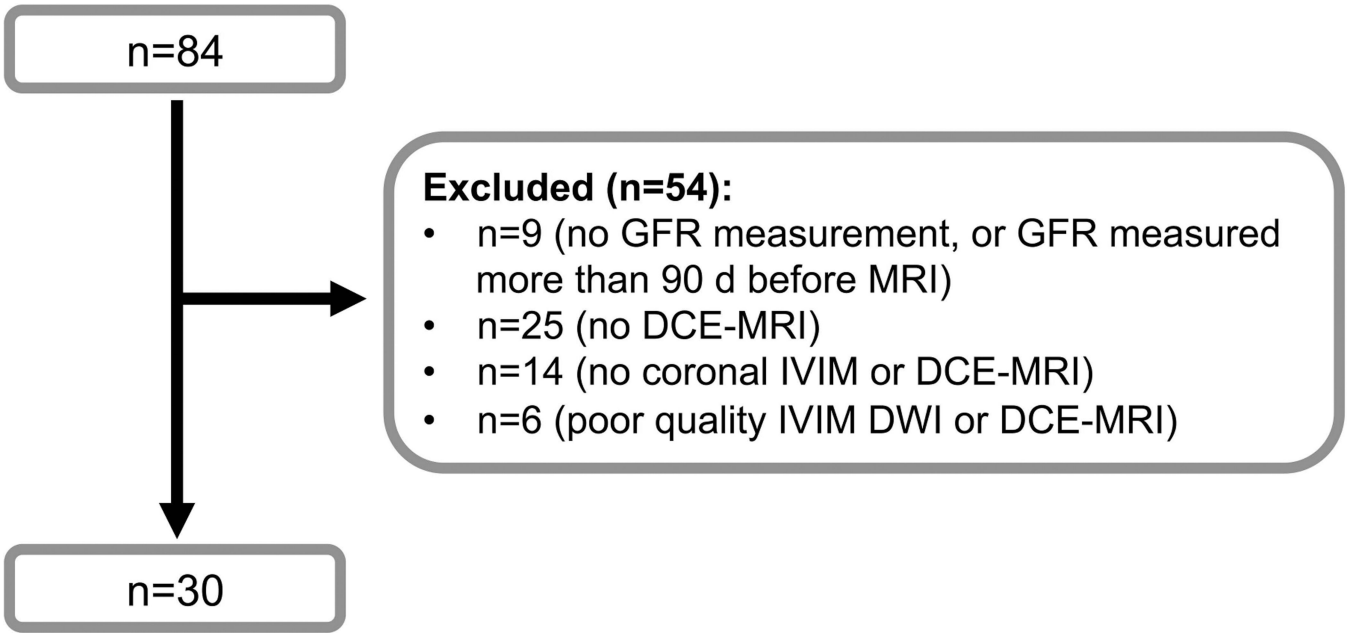

Fig. 1.

Flow-chart showing selection of patients for renal DCE-MRI and IVIM-DWI analysis. Patients were selected according to coronal IVIM and DCE-MRI orientation, and an interval between serum creatinine measurement and MRI <90 days.

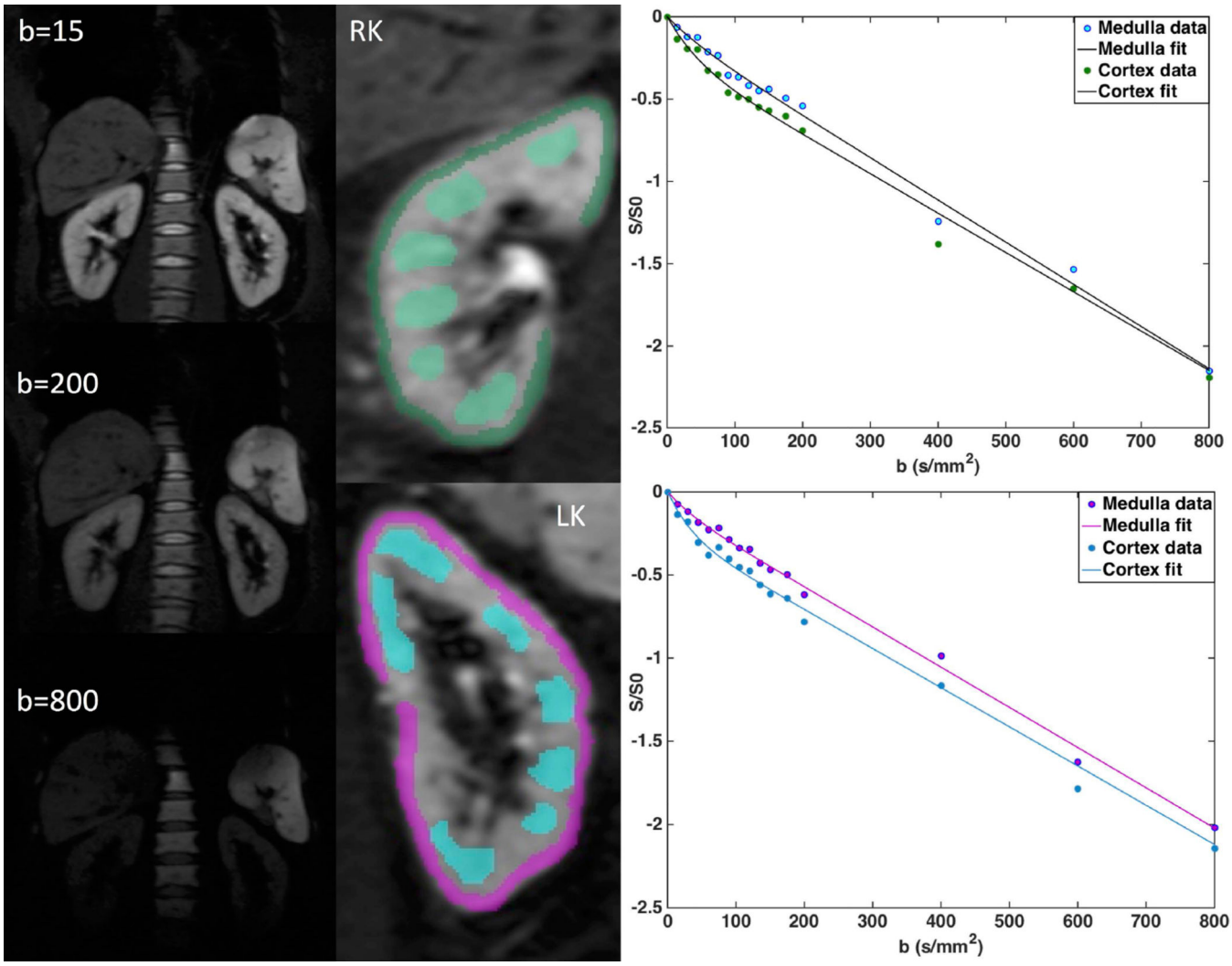

Fig. 2.

Left: IVIM-DWI abdominal images for b-values 15, 200 and 800 s/mm^2 in a 52 year-old male patient with eGFR of 112ml/min. Middle: Whole kidney, cortex and medulla ROIs outlined on b=0 and fitted IVIM signal curves. Right: Fitted IVIM-DWI curves.

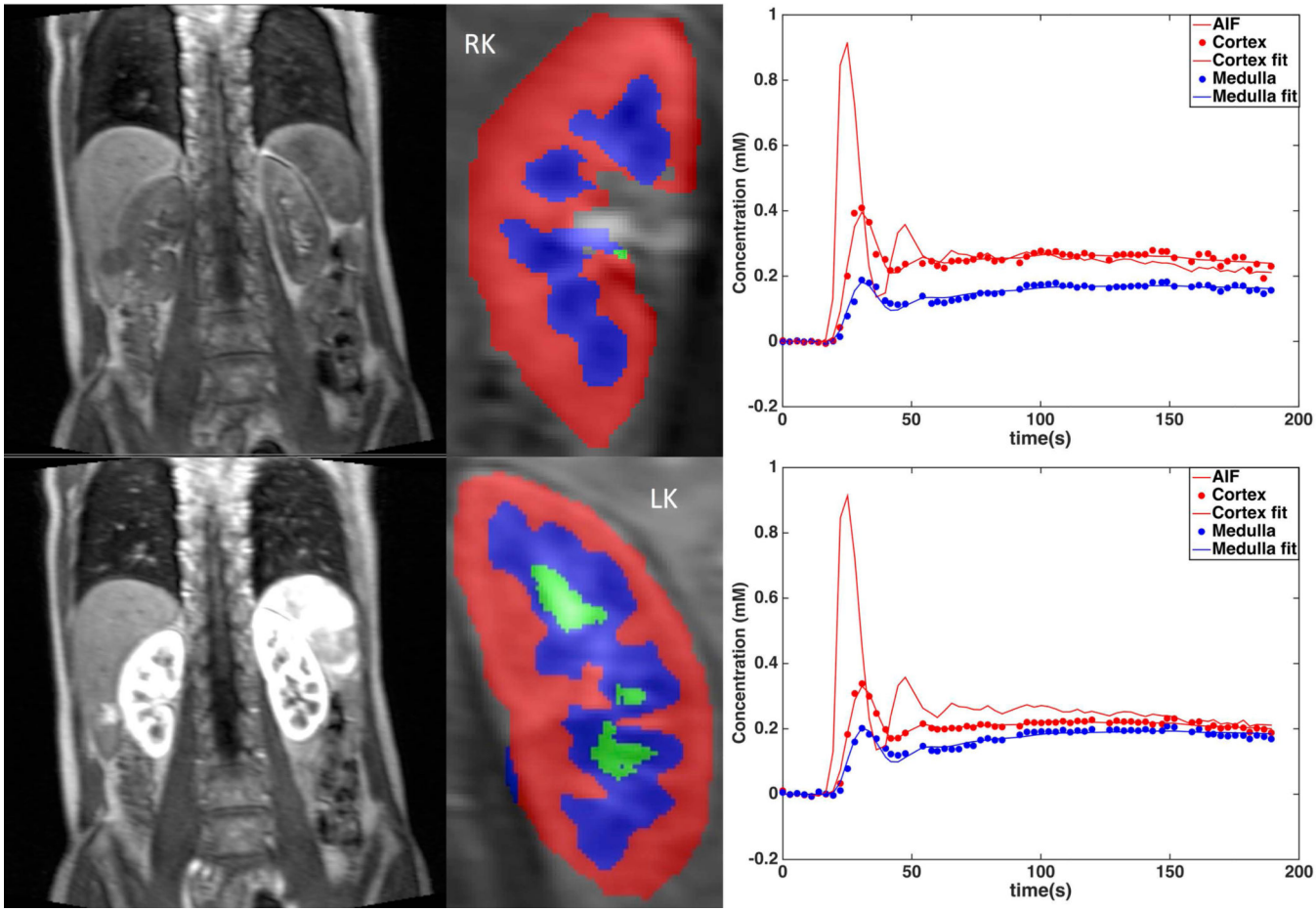

Fig. 3.

Left: Baseline (top) and arterial/cortical phase (bottom) DCE-MRI abdominal images in 64 year-old male with serum eGFR of 57 ml/min and DCE-MRI GFR of 51 ml/min. Middle: Cortex and medulla segmentation. Right: Fitted medulla and cortex concentration curves, with arterial input function (AIF).

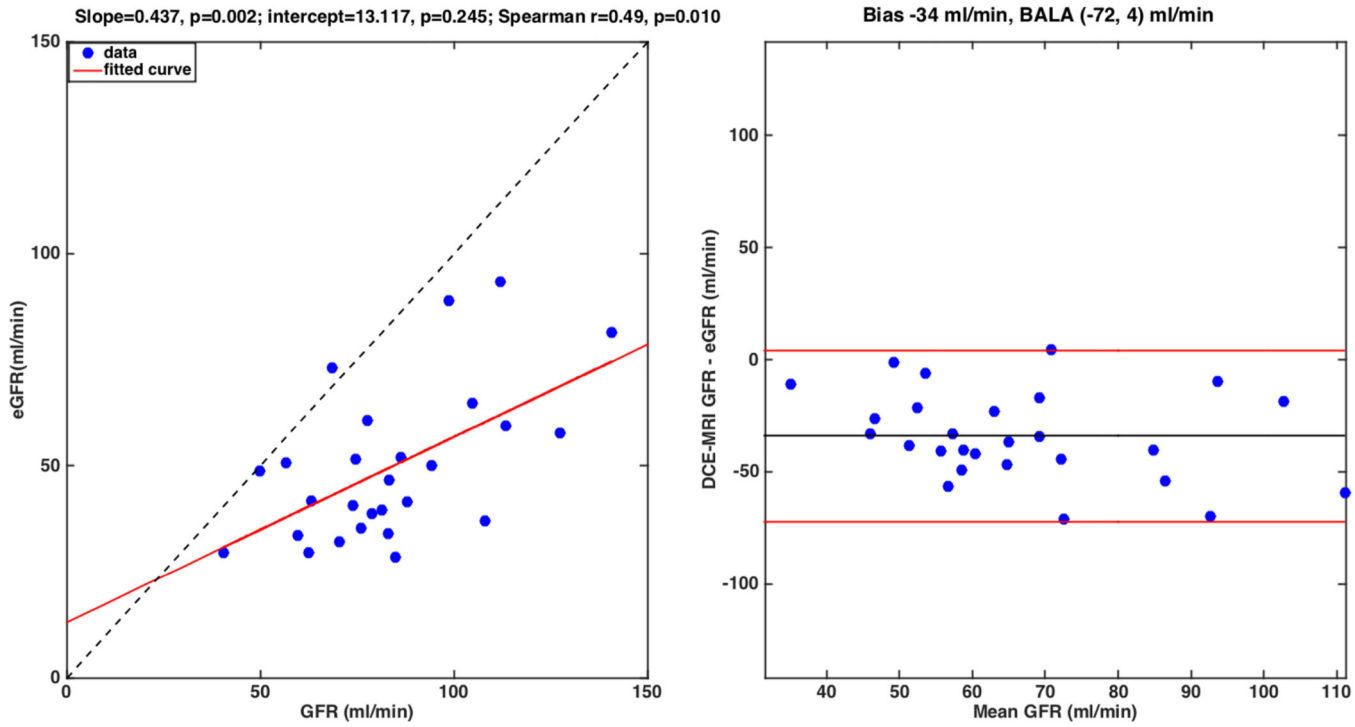

Fig. 4.

Correlation plot of DCE-MRI derived GFR with serum GFR. DCE-MRI underestimates serum GFR. Left: Correlation plot; the dotted line represents the unity line. Right: Bland-Altman plot, showing a bias of −34 ml/min and 95% limits of agreement (−72, 4) ml/min.

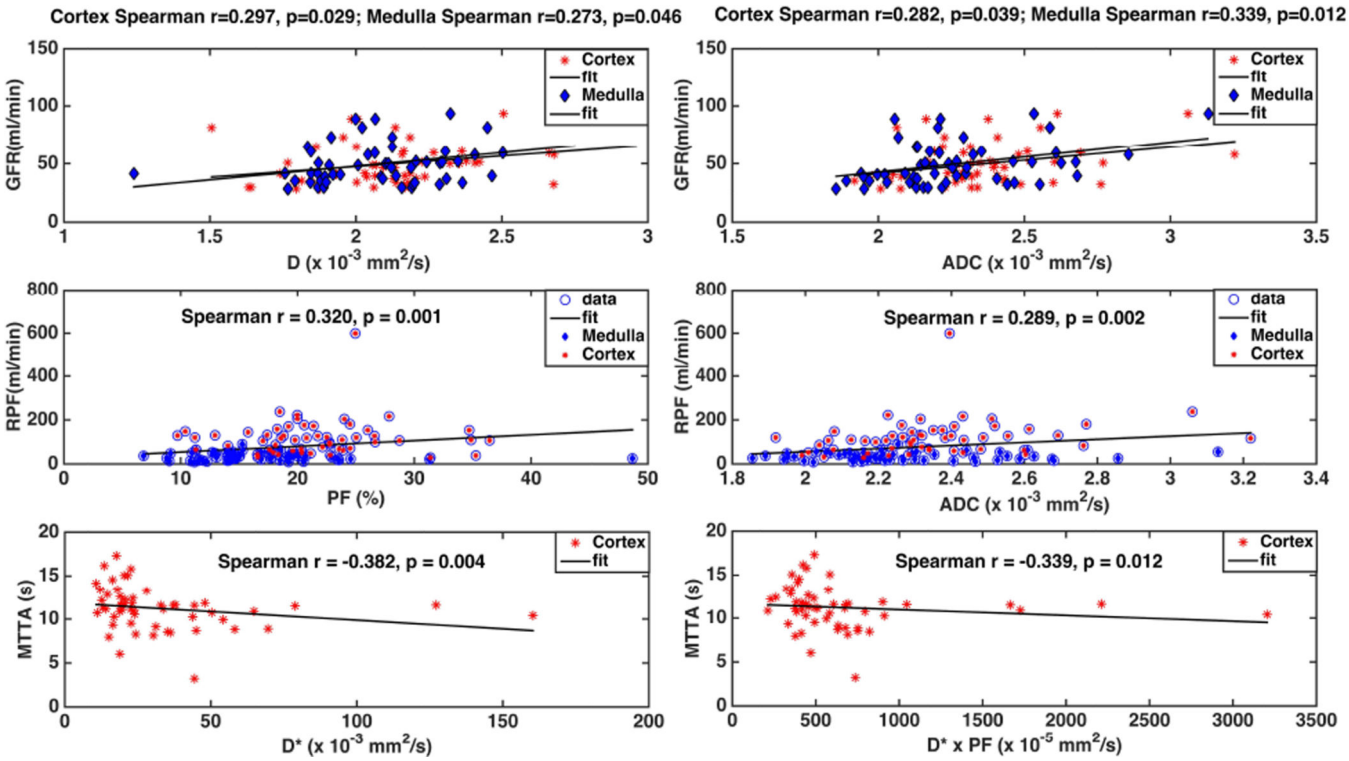

Fig. 5.

Correlation plot of IVIM-DWI metrics with DCE-MRI metrics. DCE-MRI GFR is modestly correlated to D and ADC in the cortex and medulla (top). Perfusion fraction (PF) and apparent diffusion coefficient (ADC) are moderately correlated with renal plasma flow (RPF) for pooled cortical and medullary data (middle). Mean vascular transit time (MTT_A) is negatively correlated with the pseudo-diffusion coefficient D* and its product with perfusion fraction, D*× PF (bottom).

Table 1

MRI pulse sequence parameters for T_2-weighted (T2WI) HASTE, for intravoxel-incoherent motion diffusion-weighted imaging (IVIM-DWI) and dynamic contrast-enhanced MRI (DCE-MRI).

	T2 HASTE	IVIM-DWI	DCE-MRI
Sequence type	HASTE	2D EPI	3D GRE
Orientation	Coronal	Coronal	Coronal
TR (ms)	900	3000	2.67
TE (ms)	87	74	0.94
Flip Angle	150°	90°	12°
FOV (mm^2)	350 × 350	370 × 270	400 × 400
Matrix	320 × 320	160 × 128	192 × 121
Slice thickness (mm)	7	8	4
Interpolated voxel size (mm^3)	1.1 × 1.1 × 7	2.3 × 2.9 × 8	1.04 × 1.04 × 4
Number of slices	20	17	36
Acceleration	GRAPPA R=2	GRAPPA R=2	GRAPPA R=3
Acquisition time	1 min: 14 s	10:54 ± 4:38 min	3:20 min

Table 2

IVIM-DWI parameters (mean ± SD) including perfusion fraction (PF), diffusion coefficient (D), pseudodiffusion coefficient (D*), and ADC of renal cortex and medulla measured in 30 patients. Right and left kidney metrics values are averaged.

	PF	D	D*	ADC
Cortex	21.45 ± 5.48*	2.12 ± 0.25	33.26 ± 24.04	2.36 ± 0.21
Medulla	16.42 ± 5.94	2.08 ± 0.21	38.56 ± 18.94	2.27 ± 0.22
p^	**$1.8\ 10^{-6}$**	0.5	0.13	**0.02**

^Mann-Whitney test (significant p-values are bolded)

PF: perfusion fraction (%), D: diffusion coefficient (10^{-3} mm^2/s), D*: pseudo diffusion coefficient (10^{-3} mm^2/s), ADC: apparent diffusion coefficient (10^{-3} mm^2/s)

Table 3

Estimated renal perfusion and flow parameters measured with DCE-MRI. Values represent the mean of parameters in the right and left kidney, except for global GFR, which is the sum of right and left kidney GFR. Whole kidney MTT= MTT_A+ MTT_P+ MTT_L. Whole kidney RPF is the sum of medulla and cortex RPF. MTT_A: vascular compartment MTT, MTT_P: proximal tubule MTT, and MTT_L: loop of Henle MTT.

	RPF (ml/min)	MTT (s)	GFR (ml/min)
Kidney	150.21 ± 85.57	117.88 ± 27.20	49.64 ± 17.97
	RPF (ml/min)	**MTT_A (s)**	**MTT_P (s)**
Cortex	121.06 ± 73.37 *	11.19 ± 2.04	69.76 ± 21.19
	RPF (ml/min)	**MTT_L (s)**	
Medulla	33.91 ± 16.79	39.71 ± 12.55	

* Denotes significantly higher values (Mann-Whitney test, $p < 0.05$).

Table 4

Coefficient of variation (CV, in %) denoting variability of renal IVIM-DWI parameters in MRI exams repeated within 7 days (n=4) and between right and left kidney at initial exam (n=30).

Test-retest CV (%) n=4				
	PF	**D**	**D***	**ADC**
Cortex	22.4	7.0	22.9	2.6
Medulla	22.3	5.8	26.3	3.5
Right-left kidney CV (%) n=30				
	PF	**D**	**D***	**ADC**
Cortex	14.6	6.4	26.85	5.6
Medulla	15.4	6.5	35.5	5.5

Table 5

Coefficient of variation (CV, in %) denoting variability of renal DCE-MRI parameters in MRI exams repeated within 7 days (n=2) and between right and left kidney at initial exam (n=27).

	Test-retest CV (%) n=2		
	RPF (ml/min)	**MTT (s)**	**GFR (ml/min)**
Kidney	22.7	15.7	22.4
	RPF (ml/min)	**MTT_A (s)**	**MTT_P (s)**
Cortex	25.5	3.9	9.5
	RPF (ml/min)	**MTT_L (s)**	
Medulla	16.3	23.5	
	Right-left kidney CV (%) n=27		
	RPF (ml/min)	**MTT (s)**	**GFR (ml/min)**
Kidney	25.2	15.8	N/A
	RPF (ml/min)	**MTT_A (s)**	**MTT_P (s)**
Cortex	24.0	11.4	23.6
	RPF (ml/min)	**MTT_L (s)**	
Medulla	17.4	20.9	